

# A Study of ISM of Dwarf Galaxies Using HI Power Spectrum Analysis

Prasun Dutta<sup>1\*</sup>, Ayesha Begum<sup>2†</sup>, Somnath Bharadwaj<sup>1‡</sup>, and Jayaram N. Chengalur<sup>3§</sup>

<sup>1</sup> *Department of Physics and Meteorology & Centre for Theoretical Studies, IIT Kharagpur, 721 302 India.*

<sup>2</sup> *Department of Astronomy, University of Wisconsin 475 N. Charter Street Madison, WI 53706, USA*

*& Institute of Astronomy, University of Cambridge, Madingley Road, Cambridge, UK.*

<sup>3</sup> *National Centre For Radio Astrophysics, Post Bag 3, Ganeshkhind, Pune 411 007, India.*

30 May 2018

## ABSTRACT

We estimate the power spectrum of HI intensity fluctuations for a sample of 8 galaxies (7 dwarf and one spiral). The power spectrum can be fitted to a power law  $P_{\text{HI}}(U) = AU^\alpha$  for 6 of these galaxies, indicating turbulence is operational. The estimated best fit value for the slope ranges from  $\sim -1.5$  (AND IV, NGC 628, UGC 4459 and GR 8) to  $\sim -2.6$  (DDO 210 and NGC 3741). We interpret this bi-modality as being due to having effectively 2D turbulence on length scales much larger than the scale height of the galaxy disk and 3D otherwise. This allows us to use the estimated slope to set bounds on the scale heights of the face-on galaxies in our sample. We also find that the power law slope remains constant as we increase the channel thickness for all these galaxies, suggesting that the fluctuations in HI intensity are due to density fluctuations and not velocity fluctuations, or that the slope of the velocity structure function is  $\sim 0$ . Finally, for the four galaxies with “2D turbulence” we find that the slope  $\alpha$  correlates with the star formation rate per unit area, with larger star formation rates leading to steeper power laws. Given our small sample size this result needs to be confirmed with a larger sample.

**Key words:** physical data and process: turbulence-galaxy:disc-galaxies:ISM

\* Email: prasun@cts.iitkgp.ernet.in

† Email: begum@astro.wisc.edu

‡ Email: somnath@cts.iitkgp.ernet.in

§ Email: chengalu@ncra.tifr.res.in

## 1 INTRODUCTION

Evidence has been mounting in recent years that turbulence plays an important role in the physics of the ISM as well as in governing star formation. It is believed that turbulence is responsible for generating the hierarchy of structures present across a range of spatial scales in the ISM (e.g. Elmegren & Scalo 2004a; Elmegren & Scalo 2004b). In such models the ISM has a fractal structure and the power spectrum of intensity fluctuations is a power law, indicating that there is no preferred “cloud” size.

On the observational front, power spectrum analysis of HI intensity fluctuations is an important technique to probe the structure of the neutral ISM in galaxies (Lazarian 1995; Oey 2002). The power spectra of the HI intensity fluctuations in our own galaxy, the LMC and the SMC all show power law behavior (Crovisier & Dickey 1983; Green 1993; Deshpande et al. 2000; Elmegreen et al. 2001; Stanimirovic et al. 1999) which is a characteristic of a turbulent medium. Similarly, Westpfahl et al. (1999) showed that the HI distribution in several galaxies in the M81 group has a fractal distribution. Krakow et al. (1982) have estimated the power spectrum of optical intensity fluctuation for the galaxies M 81, M 51 and NGC 1365 using digitized images in different bands. The power spectra were found to show both long and short range order. Further, Willett et al. (2005) used the Fourier transform power spectra of the V and H $\alpha$  images of a sample of irregular galaxies to show that the power spectra in optical and H $\alpha$  pass-bands are also well fit by power laws, indicating that there is no characteristic mass or luminosity scale for OB associations and star complexes. Roy et al. (2009) have estimated the power spectrum of the supernovae remnants Cas A and Crab. The power spectrum is found to be power law, indicating the presence of magneto-hydrodynamic turbulence.

Recently Begum et al. (2006) have presented a visibility based formalism for determining the power spectrum of HI intensity fluctuations in galaxies with extremely weak emission. This formalism is very similar to that used for analyzing radio-interferometric observations of the Cosmic Microwave Background Radiation anisotropies (Hobson et al. 1995; White et al. 1999; Hobson & Maisinger 2002; Dickinson 2004). This formalism was first applied to a dwarf galaxy, DDO 210. Interestingly, the HI power spectrum of this extremely faint, largely quiescent galaxy was found to be a power law with the same slope ( $-2.8 \pm 0.4$ ) as that observed in much brighter galaxies. We (Dutta et al. 2008) have applied the same technique to an external spiral galaxy NGC 628 (M 74) and found a different slope ( $-1.7 \pm 0.2$ ). In this

Galaxies	DDO 210	NGC 628	NGC 3741	UGC 4459	GR 8	AND IV	KK 230	KDG 52
(1) Type	Dwarf	Spiral	Dwarf	Dwarf	Dwarf	Dwarf	Dwarf	Dwarf
(2) Distance (Mpc)	1.0	8.0	3.0	3.56	2.1	6.7	1.9	3.55
(3) Log[SFR] ( $M_{\odot}\text{yr}^{-1}$ )	>-5.42	-0.1	-2.47	-2.04	-2.46	-3.0	>-5.53	>-5.1
(4) Angular extent	5' $\times$ 4.5'	13' $\times$ 12'	27' $\times$ 12'	4.5' $\times$ 4'	4.2' $\times$ 4'	15' $\times$ 8.5'	3' $\times$ 2'	3.5' $\times$ 3'
(5) $\sigma_{obs}$ ( $\text{km s}^{-1}$ )	6.5(1.0)	8.5(1.5)	$\sim 8.0$	9.0(1.6)	9.0(0.8)	$\sim 8.0$	7.5(0.5)	9.0(1.0)
(6) $i_{HI}$	26.0°	6.5°	68.0°	30.0°	27.0°	55.0°	50.0°	23.0°
(7) References	3, 6	1,8	4, 6	5,6	2, 6	7, 6	5, 6	5, 6

**Table 1.** 1- Kamphuis & Briggs (1992), 2- Begum & Chengalur (2003), 3- Begum & Chengalur (2004), 4- Begum et al. (2007), 5- Begum et al. (2006), 6- Begum et al. (2008), 7- Chengalur et al. 2009 (in preparation)8 - Persic & Rephaeli (2007)

paper we use the same formalism to measure the power spectrum of HI intensity fluctuation for a sample of 6 more dwarf galaxies. For completeness, we also include the existing results for DDO 210 and NGC 628, and search for correlations with other galaxy properties, e.g, the star formation rate (SFR). Any detected correlation would provide insights into the nature of turbulence in the ISM. In section 2 we discuss the galaxies in our sample. In section 3. we discuss the power spectrum estimator used in our work. In section 4, we perform simulations to support the analytical results obtained in section 3. The method of analysis is discussed in section 5. In the last section we present our results and conclusions.

## 2 THE GALAXY SAMPLE

We briefly discuss some of the relevant properties of the galaxies in our sample. A few of the galaxy parameters are also summarized in Table 1 which contains - Row(1): type of the galaxy; Row(2): distance in Mpc; Row(3): Log[SFR] in  $M_{\odot}\text{yr}^{-1}$  measured from  $H\alpha$  emission; Row(4): angular extent of the galaxy calculated from Moment 0 map at HI column density  $10^{19}$  atoms  $\text{cm}^{-2}$ ; Row(5): velocity dispersion ( $\text{km s}^{-1}$ ), Row(6): inclination in HI and Row(7): references.

### DDO 210

DDO 210 is the faintest ( $M_B \sim -10.9$ ) relatively close (at a distance  $950 \pm 50$  kpc; Lee et al. 1999) gas-rich member of the Local Group. The HI disc of the galaxy is nearly face-on. On large scales, the HI distribution is not axisymmetric; the integrated HI column density contours are elongated towards the east and south. No  $H\alpha$  emission was detected indicating a lack of on-going star formation in the galaxy. Distance to this galaxy is estimated to be  $950 \pm 50$  kpc in Lee et al. (1999).

**NGC 628**

NGC 628 (M74) is a nearly face-on SA(s)c spiral galaxy with an inclination angle in the range  $6^\circ$  to  $13^\circ$  (Kamphuis & Briggs 1992). It has a very large HI disk extending out to more than 3 times the Holmberg diameter. Elmegreen et al. (2006) have found a scale-free size and luminosity distribution of star forming regions in this galaxy, indicating turbulence to be functional here. The distance to this galaxy is uncertain with previous estimates ranging from 6.5 Mpc to 10 Mpc. Sharina et al. (1996) estimated a distance of  $7.8 \pm 0.9$  Mpc from the brightest blue star in the galaxy. This distance estimate matches with an independent photometric distance estimate by Sohn & Davidge (1996). In a recent study Vinkó et al. (2004) inferred the distance to be  $6.7 \pm 4.5$  Mpc by applying the expanding photosphere method to the hyper novae SN2002ap. In this paper, we adopt the photometric distance of 8.0 Mpc for this galaxy.

**NGC 3741**

NGC 3741 is a nearby dwarf irregular galaxy ( $M_B \sim -13.13$ ) with a gas disk that extends to  $\sim 8.8$  times the Holmberg radius (Begum et al. 2005, 2007). The galaxy is fairly edge-on with kinematical inclination varying from  $\sim 58^\circ - 70^\circ$ . NGC 3741 appears to have a HI bar and is very dark matter dominated with a dark to luminous mass ratio of  $\sim 149$ . Further, this galaxy is undergoing significant star formation in the center. An interplay between the neutral ISM and star formation in this galaxy is studied in detail in Begum et al. (2007). The rotation curve flattens beyond  $300''$  to a value  $\sim 50 \text{ km s}^{-1}$  (Gentile et al. 2007). They find that the ISM in this galaxy shows radial motion of  $\sim 5 - 13 \text{ km s}^{-1}$ . Karachentsev et al. (2004) have estimated the distance to this galaxy as  $3.0 \pm 0.3$  Mpc using the tip of the red giant branch (TRGB) method.

**UGC 4459**

The faint dwarf ( $M_B \sim -13.37$ ) galaxy UGC 4459 is a member of the M 81 group of galaxies. It is fairly isolated from its nearest neighbor UGC 4483 at a projected distance of  $3.6^\circ$  ( $\sim 223$  kpc) and a velocity difference  $135 \text{ km s}^{-1}$ . UGC 4459 is a relatively metal poor galaxy, with  $12 + \log(\text{O}/\text{H}) \sim 7.62$  (Kunth & Östlin 2000). The optical appearance of this galaxy is dominated by bright blue clumps, which emits copious amount of  $\text{H}\alpha$ , indicating high star formation. The velocity field of UGC 4459 shows a large scale gradient across the galaxy

with an average of  $\sim 4.5 \text{ km s}^{-1} \text{ kpc}^{-1}$ , though this gradient is not consistent with that expected from a systematic rotating disk. This galaxy has a TRGB distance of 3.56 Mpc (Karachentsev et al. 2004).

### **GR 8**

This is a faint ( $M_B \sim -12.1$ ) dwarf irregular galaxy with very unusual HI kinematics (Begum & Chengalur (2003)). The HI distribution in the galaxy is very clumpy, and shows substantial diffuse, extended gas. The high density HI clumps in the galaxy are associated with optical knots. In optical it has a patchy appearance with the emission dominated by bright blue knots which are sites of active star formation (Hodge 1967). Both radial and circular motions are present in this galaxy. It also possesses a faint extended emission in  $\text{H}\alpha$ . The distance to this galaxy is estimated to be 2.10 Mpc (Karachentsev et al. 2004).

### **AND IV**

This is a dwarf irregular galaxy with a moderate surface brightness ( $\bar{\mu}_V \sim 24$ ) and a very blue colour ( $V - I \leq 0.6$ ) (Ferguson et al. 2000). It is at a projected distance of  $40'$  from the center of M 31 (Merrett et al. 2006) and has a very low ongoing SFR of  $\sim 0.001 M_\odot \text{ yr}^{-1}$ . Its HI disk extends to  $\sim 6$  times the Holmberg diameter and also shows large scale, purely gaseous spiral arms Chengalur et al. 2008 (in preparation). The distance to this galaxy is estimated to be  $6.7 \pm 1.5$  Mpc (Ferguson et al. 2000).

### **KK 230**

KK 230, the faintest ( $M_B \sim -9.55$ ) dwarf irregular galaxy in our sample, lies at the periphery of the Canes Venatici I cloud of galaxies (Karachentsev et al. 2004). The velocity field shows a gradient in the direction roughly perpendicular to the HI and optical major axis with a magnitude of  $\sim 6 \text{ km s}^{-1} \text{ kpc}^{-1}$  (Begum et al. 2006). There is no measurable ongoing star formation in this galaxy as inferred from the absence of any detectable  $\text{H}\alpha$  emission. Karachentsev et al. (2004) have found a tidal index of  $-1.0$  indicating the galaxy to be fairly isolated. They have estimated the TRGB distance to be 1.9 Mpc.

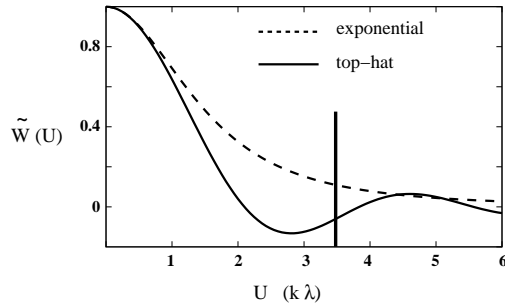


**Figure 1.**  $\tilde{W}(U)$  for top-hat and exponential window functions for  $\theta_0 = 1'$ . The vertical line marks  $\theta_0^{-1}$ . Note that the FWHM of the two window functions are nearly the same and both window functions have a very small value for  $U > \theta_0^{-1}$ .

## KDG 52

KDG 52 (also called M 81DwA), another member of the M81 group, is a faint dwarf galaxy ( $M_B \sim -11.49$ ) with a clumpy HI distribution in a broken ring surrounding the optical emission (Begum et al. 2006). The HI hole is not exactly centered around the optical emission. This galaxy does not have any detectable ongoing star formation. The distance to this galaxy is estimated to be 3.55 Mpc (Karachentsev et al. 2004) derived from the TRGB method.

## 3 A VISIBILITY BASED POWER SPECTRUM ESTIMATOR

The specific intensity of HI emission from a galaxy can be modeled as

$$I_\nu(\vec{\theta}) = W_\nu(\vec{\theta}) [\bar{I}_\nu + \delta I_\nu(\vec{\theta})]. \quad (1)$$

Here  $\vec{\theta}$  is the angle on the sky measured in radians from the center of the galaxy. We assume that the galaxy subtends a small angle so that  $\vec{\theta}$  may be treated as a two dimensional (2D) planar vector on the sky. The HI specific intensity is modeled as the sum of a smooth component and a fluctuating component. Typically,  $I_\nu(\vec{\theta})$  is maximum at the center and declines with increasing  $\theta$ . We model this through a window function  $W_\nu(\vec{\theta})$  which is defined so that  $W_\nu(0) = 1$  at the center and has values  $1 \geq W_\nu(\vec{\theta}) \geq 0$  elsewhere. This multiplied by  $\bar{I}_\nu$  gives the smooth component of the specific intensity. For a face-on galaxy, the window function  $W_\nu(\vec{\theta})$  corresponds to the galaxy's radial profile.

Consider a galaxy of angular radius  $\theta_0$ . In our analysis we consider two different models for the window function of such a galaxy. In the ‘‘top-hat’’ model it is assumed that the specific intensity has a constant value within a circular disk of radius  $\theta_0$ , and it abruptly falls to 0 outside. The window function, in this case, is a Heaviside step function

$$W_\nu(\vec{\theta}) = \Theta(\theta_0 - \theta) \tag{2}$$

In the ‘‘exponential’’ model the window function has the form

$$W_\nu(\vec{\theta}) = \exp\left(-\frac{\sqrt{12}\theta}{\theta_0}\right). \tag{3}$$

where it falls exponentially away from the center.

It is also possible to use  $W_\nu(\vec{\theta})$  to define a normalized window function  $W_\nu^N(\vec{\theta})$  such that  $\int d^2\theta W_\nu^N(\vec{\theta}) = 1$ . The second moment of  $\theta$  defined as  $\int d^2\theta \theta^2 W_\nu^N(\vec{\theta})$  provides a good estimate of the angular extent of the window function. Here we have used the condition that this should have the same value  $\theta_0^2/2$  for all models of the window function, to determine the width of the exponential window function in terms of  $\theta_0$ . Throughout we have assumed  $\theta_0 \ll 1$  radian.

We express the fluctuating component of the specific intensity as  $W_\nu(\vec{\theta}) \delta I_\nu(\vec{\theta})$ . Here  $\delta I_\nu(\vec{\theta})$  is a stochastic fluctuation which is assumed to be statistically homogeneous and isotropic. The HI emission traces these fluctuations modulated by the window function which quantifies the large-scale HI distribution. In this paper we would like to use radio-interferometric observations to quantify the statistical properties of the fluctuations  $\delta I_\nu(\vec{\theta})$ . These fluctuations are believed to be the outcome of turbulence in the inter-stellar medium.

The visibility  $\mathcal{V}_\nu(\vec{U})$  recorded in radio-interferometric observations is the Fourier transform of the product of the antenna primary beam pattern  $A_\nu(\vec{\theta})$  and the specific intensity distribution of the galaxy.

$$\mathcal{V}_\nu(\vec{U}) = \int d\vec{\theta} e^{-i2\pi\vec{U}\cdot\vec{\theta}} A_\nu(\vec{\theta}) I_\nu(\vec{\theta}) \tag{4}$$

Here  $\vec{U}$  refers to a baseline, the antenna separation measured in units of the observing wavelength  $\lambda$ . It is common practice to express  $\vec{U}$  in units of kilo wavelength (k $\lambda$ ). Throughout this paper we follow the usual radio inteferometric convention and express  $\vec{U}$  in units of kilo wavelengths (k $\lambda$ ).

The angular extent of the galaxies that we consider here is much smaller than the primary beam, and the effect of the primary beam may be ignored. We then have

$$\mathcal{V}_\nu(\vec{U}) = \tilde{W}(\vec{U}) \tilde{I}_\nu + \tilde{W}(\vec{U}) \otimes \tilde{\delta I}_\nu(\vec{U}) + \mathcal{N}_\nu(\vec{U}) \tag{5}$$

where the tilde  $\tilde{\phantom{x}}$  denotes the Fourier transform of the corresponding quantity and  $\otimes$  denotes a convolution. In addition to the signal, each visibility also contains a system noise contribution  $\mathcal{N}_\nu(\vec{U})$  which we have introduced in eq. (5). The noise in each visibility is a Gaussian random variable and the noise in the visibilities at two different baselines  $\vec{U}$  and  $\vec{U}'$  is uncorrelated.

The Fourier transform of the normalized window functions are

$$\tilde{W}_\nu(\vec{U}) = 2 \frac{J_1(2\pi\theta_0 U)}{2\pi\theta_0 U} \quad (6)$$

and

$$\tilde{W}_\nu(\vec{U}) = \frac{1}{[1 + \pi^2\theta_0^2 U^2/3]^{3/2}} \quad (7)$$

for the top-hat and exponential models respectively. Here  $J_1(x)$  is the Bessel function of order 1. These functions, shown in Figure 1, have the property that they peak around  $U = 0$  and fall off rapidly for  $U \gg \theta_0^{-1}$ . This is a generic property of the window function, not restricted to just these two models. At baselines  $U \gg \theta_0^{-1}$  we may safely neglect the first term in eq. (5) whereby

$$\mathcal{V}_\nu(\vec{U}) = \tilde{W}(\vec{U}) \otimes \delta\tilde{I}_\nu(\vec{U}) + \mathcal{N}_\nu(\vec{U}) \quad (8)$$

We use the power spectrum of HI intensity fluctuations  $P_{\text{HI}}(U)$  defined as

$$\langle \delta\tilde{I}_\nu(\vec{U}) \delta\tilde{I}_\nu^*(\vec{U}') \rangle = \delta_D^2(\vec{U} - \vec{U}') P_{\text{HI}}(U) \quad (9)$$

to quantify the statistical properties of the intensity fluctuations. Here,  $\delta_D^2(\vec{U} - \vec{U}')$  is a two dimensional Dirac delta function. The angular brackets here denote an ensemble average over different realizations of the stochastic fluctuation. In reality, it is not possible to evaluate this ensemble average because a galaxy presents us with only a single realization. In practice we evaluate an angular average over different directions of  $\vec{U}$ . This is expected to provide an estimate of the ensemble average for a statistically isotropic fluctuation.

The square of the visibilities can, in principle, be used to estimate  $P_{\text{HI}}(U)$

$$\langle \mathcal{V}_\nu(\vec{U}) \mathcal{V}_\nu^*(\vec{U}) \rangle = |\tilde{W}_\nu(\vec{U})|^2 \otimes P_{\text{HI}}(\vec{U}) + \langle |\mathcal{N}_\nu(\vec{U})|^2 \rangle \quad (10)$$

and this has been used in several earlier studies (Crovisier & Dickey 1983; Green 1993; Lazarian 1995). This technique has limited utility to observations where the HI signal in each visibility exceeds the noise. This is because the last term  $\langle |\mathcal{N}_\nu(\vec{U})|^2 \rangle$ , which is the noise variance introduces a positive bias in estimating the power spectrum. The noise bias can be orders of magnitude larger than the power spectrum for the faint external galaxies considered here. In principle, the noise bias may be separately estimated using line-free channels and subtracted. In practice this is extremely difficult owing to uncertainties in the bandpass response which restrict the noise statistics to be estimated with the required accuracy. Attempts to subtract out the noise-bias have shown that it is not possible to do this at the level of accuracy required to detect the HI power spectrum (Begum 2006).



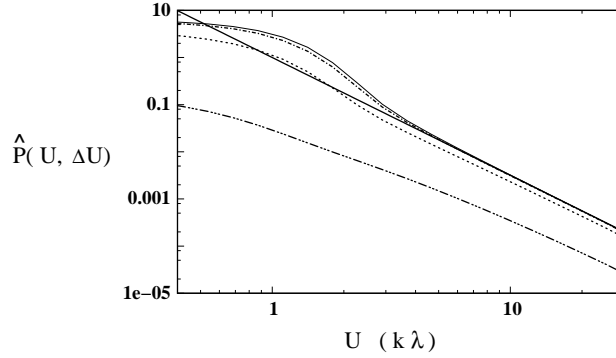


**Figure 2.** This shows the convolution (eqn. 11) of a power law  $P_{\text{HI}}(U) = U^{-2.5}$  with the product of two exponential window functions (eqn. 7) with  $\theta_0 = 1'$  ( $(\pi\theta_0)^{-1} \approx 1 \text{ k}\lambda$ ). The bold solid curve shows the original power law and the thin solid curve shows  $P_{\text{HI}}(\vec{U}, \Delta\vec{U})$  for  $\Delta\vec{U} = 0$ . The dashed curves are for  $|\Delta\vec{U}| = 0.2, 1.0$  and  $3.0 \text{ k}\lambda$  respectively from top to bottom. The direction of  $\Delta\vec{U}$  is parallel to that of  $\vec{U}$ . Note that  $P_{\text{HI}}(\vec{U}, 0.2) \approx P_{\text{HI}}(\vec{U}, 0)$  and the correlation between two different visibilities is small for  $|\Delta\vec{U}| > (\pi\theta_0)^{-1}$ .

The problem of noise bias can be avoided by correlating visibilities at two different baselines for which the noise is expected to be uncorrelated. We define the power spectrum estimator

$$\begin{aligned} \hat{P}_{\text{HI}}(\vec{U}, \Delta\vec{U}) &= \langle \mathcal{V}_\nu(\vec{U}) \mathcal{V}_\nu^*(\vec{U} + \Delta\vec{U}) \rangle \\ &= \int d^2U' W_\nu(\vec{U} - \vec{U}') W_\nu^*(\vec{U} + \Delta\vec{U} - \vec{U}') P_{\text{HI}}(\vec{U}') \end{aligned} \quad (11)$$

Since  $\tilde{W}(\vec{U})$  falls off rapidly for  $U \gg \theta_0^{-1}$  (Figure 1), the window functions  $W_\nu(\vec{U} - \vec{U}')$  and  $W_\nu^*(\vec{U} + \Delta\vec{U} - \vec{U}')$  in eqn. (11) have a substantial overlap only if  $|\Delta\vec{U}| < (\pi\theta_0)^{-1}$ . Visibilities at two different baselines will be correlated only if  $|\Delta\vec{U}| < (\pi\theta_0)^{-1}$ , and not beyond (Figure 2). In our analysis we restrict the difference in baselines to  $|\Delta\vec{U}| \ll (\pi\theta_0)^{-1}$  so that  $\tilde{W}_\nu(\vec{U} + \Delta\vec{U} - \vec{U}') \approx \tilde{W}_\nu(\vec{U} - \vec{U}')$  and the estimator  $\hat{P}_{\text{HI}}(\vec{U}, \Delta\vec{U})$  no longer depends on  $\Delta\vec{U}$  (Figure 2). We then use the visibility correlation estimator

$$\begin{aligned} \hat{P}_{\text{HI}}(\vec{U}) &= \langle \mathcal{V}_\nu(\vec{U}) \mathcal{V}_\nu^*(\vec{U} + \Delta\vec{U}) \rangle \\ &= \int d^2U' |W_\nu(\vec{U} - \vec{U}')|^2 P_{\text{HI}}(\vec{U}'). \end{aligned} \quad (12)$$

The measured visibility correlation  $\hat{P}_{\text{HI}}(\vec{U})$  will, in general, be complex. The real part is the power spectrum of HI intensity fluctuations convolved with the square of the window function. A further simplification is possible at large baselines  $U \gg \theta_0^{-1}$ , provided  $|\tilde{W}_\nu(U)|^2$  decays much faster than the variations in  $P_{\text{HI}}(U)$ . We then have

$$\hat{P}_{\text{HI}}(\vec{U}) = C P_{\text{HI}}(\vec{U}) \quad (13)$$

where  $C = \int |W_\nu(U)|^2 d^2U$  is a constant.

We use the real part of the estimator  $\hat{P}_{\text{HI}}(\vec{U})$  to estimate the power spectrum  $P_{\text{HI}}(U)$ . Our interpretation is restricted to the  $U$  range  $U \gg (\pi\theta_0)^{-1}$  where the convolution in eq.

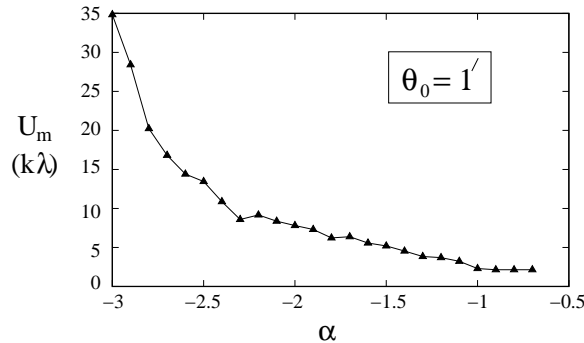


**Figure 3.** This shows how  $U_m$  changes with  $\alpha$  for an exponential window function with  $\theta_0 = 1'$ . Note that the discontinuities seen in the plot appear to be genuine features and not numerical artifacts, though the cause of these features is not clear at present.

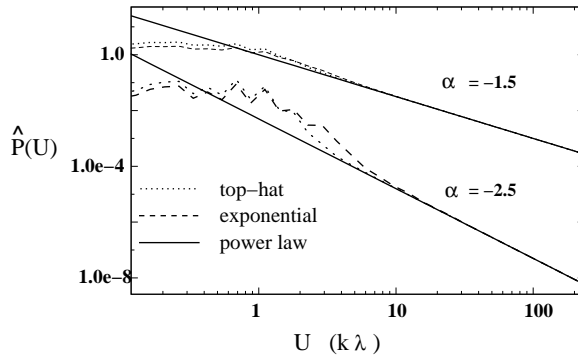


**Figure 4.** Effect of window function modifies the power spectrum differently for different power law exponents.

(12) does not affect the shape of the power spectrum and eq. (13) is a valid approximation. In order to estimate the  $U$  range where this approximation is valid we have numerically evaluated eq. (11) assuming  $P_{\text{HI}}(U)$  to be a power law  $P_{\text{HI}}(U) = AU^\alpha$ . Figure 4 shows the results for both the top-hat and the exponential models with  $\theta_0 = 1'$  ( $\theta_0^{-1} = 3.4 \text{ k}\lambda$ ) and  $\alpha = -1.5$  and  $-2.5$  which roughly spans the range of slopes that we encounter in our galaxy sample. Using  $U_m$  to denote the value (in  $\text{k}\lambda$ ) where the deviation from the original power law is 10%, we find that for the top-hat and exponential models respectively  $U_m$  has values (3.1, 5.3) for  $\alpha = -1.5$  and (4.8, 13.0) for  $\alpha = -2.5$ . Note that  $U_m$  depends on two parameters, namely  $\alpha$  and  $\theta_0$ . Figure 3 shows how  $U_m$  changes with  $\alpha$  for the exponential model with  $\theta_0 = 1'$ . For other values of  $\theta_0$  we scale the value of  $U_m$  in Figure 3 using  $U_m \propto \theta_0^{-1}$ . For a given power law index, the estimator  $\hat{P}_{\text{HI}}(\vec{U})$  gives a direct estimate of the power spectrum for  $U \geq U_m$ .

The estimator  $\hat{P}_{\text{HI}}(\vec{U})$  also has a small imaginary part that arises from the HI power spectrum because the assumption that  $\tilde{W}_\nu(\vec{U} + \Delta\vec{U} - \vec{U}') \approx \tilde{W}_\nu(\vec{U} - \vec{U}')$  is not strictly valid.

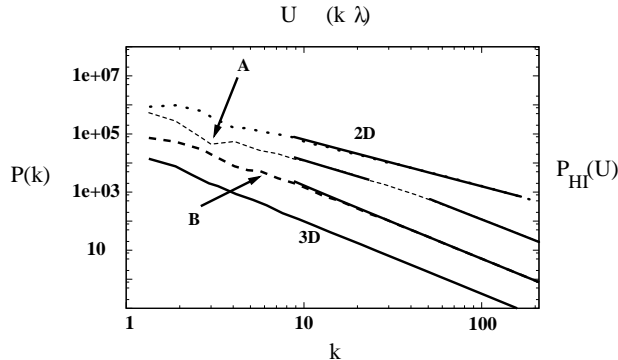


**Figure 5.** The 3D and 2D power spectrum  $P(k)$ . The simulated HI power spectrum  $P_{\text{HI}}(U)$  for the thin (A) and thick (B) disk without the radial profile are also shown. The  $P(k)$  and  $k$  values (left and bottom axes) have been arbitrarily scaled to match the  $P_{\text{HI}}(U)$  and  $U$  axes (top and right). The power-law fits are shown by solid lines. The different curves have been plotted with arbitrary offsets to make them distinguishable.

We use the requirement that the imaginary part of  $\hat{P}_{\text{HI}}(\vec{U})$  should be small compared to the real part as a self-consistency check to determine the range of validity of our formalism.

The real and imaginary parts of the measured value of the estimator  $\hat{P}_{\text{HI}}(\vec{U})$  both have uncertainties arising from (1.) the sample variance and (2.) the system noise. The sample variance is  $[\hat{P}_{\text{HI}}(\vec{U})/\sqrt{N_E}]^2$ , where  $N_E$  is the number of independent estimates. We assume that in the u-v plane the HI signal is uncorrelated beyond 1.5 times the FWHM of  $|\tilde{W}_v^2(U)|^2$ . We use this to determine  $N_E$  from the u-v coverage of our observations. The system noise variance is  $\sigma^4/N_P$  where  $\sigma^2$  is the variance of the individual visibilities in the data and  $N_P$  is the number of visibility pairs that contribute to each visibility correlation. We add both these contributions to determine the  $1 - \sigma$  error-bars. The reader is referred to Section 3.2 of Ali et al. (2008) for further details of the error estimation.

## 4 SIMULATION

We have carried out simulations to assess the impact of the overall galaxy structure on our estimates of the power spectrum of HI intensity fluctuations. The starting point is a three dimensional (3D)  $512^3$  cubic mesh, labeled using coordinates  $\vec{r}$ , on which we generate a statistically homogeneous and isotropic Gaussian random field  $\hat{h}(\vec{r})$  with power spectrum  $P(k) = Ck^\gamma$ . We have used  $\gamma = -2.5$  throughout our simulations, the results can be easily generalized to other  $\gamma$  values. The 3D power spectrum is shown in Figure 5. For reference we also show the two dimensional (2D) power spectrum of  $\hat{h}(\vec{r})$  evaluated on a  $512^2$  planar section of the cubic mesh. As expected, the 2D power spectrum also is a power law with

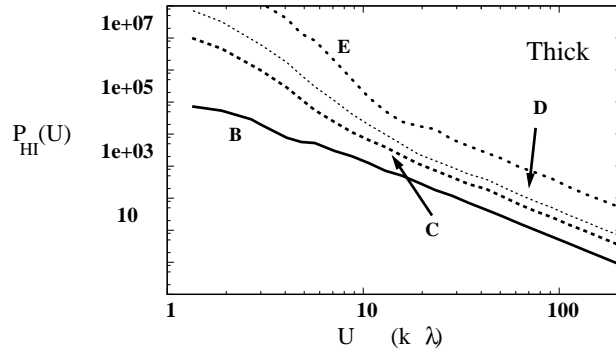


**Figure 6.** The simulated HI power spectrum for the face-on thick disk with (B) no radial profile, and (C),(D) with radial profile using  $R = 0.35, 0.7$  respectively. (E) is same as (C) with the disk tilted at  $60^\circ$ . The different curves have been plotted with arbitrary offsets to make them distinguishable.

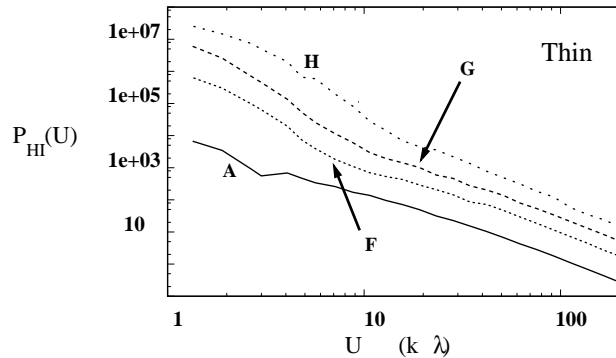


**Figure 7.** The simulated HI power spectrum for the face-on thin disk with (A) no radial profile, and (F),(G) with radial profile using  $R = 0.35, 0.7$  respectively. (H) is same as (F) with the disk tilted at  $60^\circ$ . The different curves have been plotted with arbitrary offsets to make them distinguishable.

$P(k) \propto k^{\gamma+1}$ . In all cases we have generated five independent realizations of the Gaussian random field, and averaged the power spectrum over these to reduce the statistical uncertainties.

In our simulations we use the Gaussian random field  $\hat{h}(\vec{r})$  as a model for the 3D HI density fluctuations that would arise from homogeneous and isotropic 3D turbulence. The  $\hat{h}(\vec{r})$  values on a 2D section through the cube serves as a model for the HI density fluctuations in the limiting situation where we ignore the thickness of the galaxy and treat it as a 2D disk. Note that the resulting  $\hat{h}(\vec{r})$  is a statistically homogeneous and isotropic Gaussian random field on the 2D section. We use this to represent the density fluctuations that would arise from homogeneous and isotropic 2D turbulence.

We next embed a galaxy in the middle of the 3D cube. The overall, large-scale structure of the galaxy is introduced through a function  $G(\vec{r})$  so that the HI density at any position is

$G(\vec{r})[h_0 + \hat{h}(\vec{r})]$ . Here  $G(\vec{r})h_0$  is the smoothly varying component of the galaxy’s HI density and  $G(\vec{r})\hat{h}(\vec{r})$  is its fluctuating component. It is assumed that the observer’s line of sight is along the  $z$  axis. The HI density  $G(\vec{r})[h_0 + \hat{h}(\vec{r})]$  is projected on the  $x - y$  plane. We interpret the projected values as the HI specific intensity  $I_\nu(\vec{\theta})$  in the plane of the sky (eq. 1). The  $512^2$  mesh in the  $x - y$  plane of our simulation corresponds to  $4' \times 4'$  on the sky.

We first consider a face-on galaxy, and use  $G(\vec{r}) = \exp(-z^2/z_h^2)$ . This incorporates only the finite thickness of the disk which is characterized by the scale-height  $z_h$  and it ignores the galaxy’s radial profile in the plane of the disk. Note that, for  $z < z_h$  this function closely matches the function  $\text{sech}(-z^2/z_h^2)$  which is also used to model the scale-height profile (Binney & Merrifield 1998). For the scale-height, we have used the values  $z_h = 4$  and 32 mesh units which we refer to as the “thin” and “thick” disk respectively. Figure 5 shows the power spectrum of the simulated HI specific intensity  $I_\nu(\vec{\theta})$  for both these cases. We find that the HI power spectrum of the thin disk has a slope  $-2.5$ , same as the 3D power spectrum, at large  $U$ . There is a break at  $U \sim 35 \text{ k}\lambda$  which corresponds to  $1/\pi z_h$ , and the slope is  $\sim -1.9$  at smaller  $U$ . We interpret this change in the slope in terms of a transition from 3D fluctuations on scales smaller than the disk thickness (large  $U$ ) to 2D fluctuations on scales larger than disk thickness (small  $U$ ). We expect the slope to approach  $-1.5$ , the 2D slope, at very small  $U$ . Note that in our simulation it is not possible to evaluate the slope at very small  $U$  values where the sample variance is rather large. We find that the HI power spectrum of the thick disk is well fit by a single power law  $P_{\text{HI}}(U) = AU^{-2.5}$  which has the 3D slope. In this case we expect the break corresponding to the transition from 3D to 2D at  $U \sim 4 \text{ k}\lambda$ . This break lies in the sample variance dominated region which explains why we do not detect it.

We next incorporate the galaxy’s radial profile using

$$G(\vec{r}) = \exp\left[-\frac{\sqrt{12}\theta}{\theta_0}\right] \exp(-z^2/z_h^2), \quad (14)$$

where  $\theta = \sqrt{x^2 + y^2}$  is the radial coordinate in the plane of the disk. Here  $\theta$  coincides with the angle in the sky measured from the center of the galaxy. We have used  $\theta_0 = 1'$  which corresponds to 128 mesh units. Note that the radial profile used in the simulation is exactly the same as the window function  $W(\vec{\theta})$  of the exponential model introduced in the previous section. The relative amplitude of  $h_0$  and  $\hat{h}(\vec{r})$  is a free parameter which decides the respective contributions from the smooth and the fluctuating HI components. Using the ratio  $R = \sqrt{\langle \hat{h}^2 \rangle} / h_0$  of the rms. value of  $\hat{h}(\vec{r})$  to  $h_0$  to quantify this, we have carried out

simulations for  $R = 0.35$  and  $0.7$ . We have also carried out simulations where the disk is tilted, and the normal to the disk make an angle of  $60^\circ$  to the line of sight. The simulated HI power spectra are shown in Figures 6 and 7 for the thick and thin disks respectively.

We find that for a face-on disk with  $\theta_0 = 1'$ , for both the thick and thin disks, the results of our simulations are in good agreement with our analytic estimate (Section 3) which predicts that the effect of the galaxy's radial profile is contained within a limited baseline range  $U \leq U_m$ , which comes out to be  $U \leq U_m \sim 3.5 \theta_0^{-1}$ , for  $\alpha = -2.5$  (Figure 3). The HI power spectrum is insensitive to the galaxy's radial profile at  $U > U_m$ , and the shape of the power spectrum is the same whether we include the galaxy's radial profile or not. We find that the value of  $U_m$  is not very sensitive to changes in  $R$ , the ratio of the fluctuating component to the smooth component. For a disk of the same size, the value of  $U_m$  increases when the disk is tilted. The image of the disk tilted by  $60^\circ$  has an anisotropic window function  $W(\vec{\theta})$  with angular radius  $1'$  and  $0.5'$  along the major and minor axes respectively. For a tilted disk the value of  $U_m$  is determined by the smaller of the two angular diameters,  $0.5'$  in this case.

In summary, our simulations demonstrate that for baselines  $U > U_m$  the galaxy's radial profile has no effect on the power spectrum of HI fluctuations. In other words, the power spectrum would be unchanged if the same fluctuations were present in an uniform disk with no radial profile. Further, a break in the power spectrum at a  $U$  value greater than  $U_m$  is indicative of a transition from 3D to 2D at the length-scale corresponding to the scale-height  $z_h = 1/\pi U$ .

Finally, we note that we have ignored velocity fluctuations and the galaxy's rotation throughout our simulations. This would rearrange the HI emission amongst the different frequency channels. Our simulation corresponds to the situation where there is just a single frequency channel whose width encompasses the entire HI emission, and the velocities have no effect in this situation. This is justified by the results presented later in this paper (Section 6) which show that, for the galaxies in our sample, the slope of the observed HI power spectrum does not depend on the width of the frequency channel.

## 5 METHOD OF ANALYSIS

The dwarf galaxy data used here is from Giant Metrewave Radio Telescope (GMRT) observations. The details can be found in Begum et al. (2006) for UGC 4459, KDG 52 and KK 230, Begum et al. (2005) for NGC 3741, Begum & Chengalur (2003) for GR 8, Chen-

galur et al. 2008 (in preparation) for AND IV and Begum & Chengalur (2004) for DDO 210. We use Very Large Array(VLA) archival data, discussed in Dutta et al. (2008), for the spiral galaxy NGC 628.

All the data are reduced in the usual way using standard tasks in classic AIPS <sup>1</sup>. For each galaxy, after calibration the frequency channels with HI emission were identified and a continuum image was made by combining the line free channels. The continuum was hence subtracted from the data in the  $u - v$  plane using the AIPS task UVSUB.

The number of channels with HI emission ( $n$ ) is different for each galaxy. To determine if the HI power spectrum changes with the width of the frequency channel, we combine  $N$  successive channels to obtain  $n/N$  channels and perform the power spectrum analysis for different values of  $N$  in the range  $1 \leq N \leq n$ . The analysis is initially carried out for  $N = 1$ , and unless mentioned otherwise the results refer to this value.

We measure  $\hat{P}_{\text{HI}}(U)$  by correlating every visibility  $V_\nu(\vec{U})$  with all other visibilities  $V_\nu(\vec{U} + \Delta\vec{U})$  within a disk  $|\Delta\vec{U}| \ll \theta_0^{-1}$  and then average over different  $\vec{U}$  directions. Note that correlation of a visibility with itself is excluded. To increase the signal to noise ratio we further average the correlations in bins of  $U$  and over all frequency channels with HI emission.

The measured visibility correlation estimator (eq. 12) is the convolution of the actual HI power spectrum with a window function. Here we do not attempt to estimate this window function by fitting the observed HI image and then use this to deconvolve the power spectrum. Our approach is to estimate a baseline  $U_m$ , such that for  $U \geq U_m$  the effect of the convolution can be ignored. The measured visibility estimator is proportional to the HI power spectrum (eq. 13) at baselines  $U \geq U_m$ . We estimate the HI power spectrum using only this range ( $U \geq U_m$ ) where the measured visibility correlation estimator may be directly interpreted as the HI power spectrum.

Assuming an exponential window function, the value of  $U_m$  depends on the parameters  $\theta_0$  and  $\alpha$ . Note that we do not attempt to actually fit an exponential to the observed overall HI distribution and thereby determine  $\theta_0$ . The angular radius  $\theta_0$  of the galaxies in our sample is set to half the angular extent listed in Table 1. The galaxies are typically ellipses and not circular disks as assumed in Section 3. Guided by our simulations, we have used the smaller of the two angular extents in our analysis. As  $U_m \propto \theta_0^{-1}$ , choosing the smaller value gives a conservative estimate of  $U_m$ . The upper limit  $U_u$  where we have a reliable estimate of the

<sup>1</sup> NRAO Astrophysical Image Processing System, a commonly used software for radio data processing.

HI power spectrum is determined by the requirement that the real part of  $\hat{P}_{\text{HI}}(U)$  should be more than its imaginary part and also the noise in the line free channels.

The procedure that we adopt to determine the best fit power law to the HI power spectrum is as follows. We first visually identify a baseline  $U_m$  beyond which ( $U \geq U_m$ ) the visibility correlation estimator appears to be a power law in  $U$ . We then use the range  $U_m \leq U \leq U_u$  to fit a power law  $\hat{P}_{\text{HI}}(U) = A U^\alpha$ . The best fit  $\alpha$  obtained by this fitting procedure is used to obtain a revised estimate for  $U_m$  through Figure 3. The value of  $U_m$  in this figure are for  $\theta_0 = 1'$ , we use the scaling  $U_m \propto \theta_0^{-1}$  (as mentioned above,  $\theta_0^{-1}$  is taken to be the smaller value of the two angular extents for a particular galaxy) to obtain the  $U_m$  value that is appropriate for the galaxy. The power law fitting is repeated with the revised estimate of  $U_m$ . We iterate this procedure a few times till it converges. At each iteration, the best fit  $A$  and  $\alpha$  were determined through a  $\chi^2$  minimization. To test whether the impact of the window function is actually small, we have convolved the best fit power law with  $|\tilde{W}_\nu(U)|^2$ . The convolved power spectra were visually inspected to assess the deviations from the power law. The goodness of fit to the data was also estimated by calculating  $\chi^2$  for the convolved power spectrum. The final fit is accepted only after ensuring that the effect of the convolution can actually be ignored.

The values  $D/U_m$  and  $D/U_u$ , where  $D$  is the distance to the galaxy, give an estimate of the range of length-scales over which the power-law fit holds. In addition to the other parameters of the power law fit, these values are also shown in Table 2.

## 6 RESULT AND CONCLUSION

Figure 8 and 9 show the results of our analysis. The results are summarized in Table 2. We have detected the HI power spectrum of the galaxies DDO 210, NGC 628, NGC 3741, UGC 4459, GR 8 and AND IV. For these galaxies we find a range of baselines  $U$  where the real part of  $P_{\text{HI}}(U)$  estimated from the channels with HI emission is larger than the imaginary part estimated from the same channels as well as the real part estimated from the line free channels. This is not true for KK 230 and KDG 52 (and also for AND IV with  $N = n$ ), for these galaxies all three curves (Figure 9) lie within the  $1 - \sigma$  errors-bars with very small offset and the interpretation is not straight-forward. For the subsequent analysis of all the galaxies we use only the real part of  $P_{\text{HI}}(U)$  estimated from the channels with HI emission.



Galaxies	DDO 210	NGC 628	NGC 3741	UGC 4459	GR 8	AND IV	KK 230	KDG 52
(1 a) $N$	1	1	1	1	1	1	1	1
(2 a) velocity width (km s <sup>-1</sup> )	1.65	1.29	1.65	1.65	1.65	1.65	1.65	1.65
(3 a) $\alpha$	-2.3 ± 0.6	-1.6 ± 0.2	-2.2 ± 0.4	-1.8 ± 0.6	-1.1 ± 0.4	-1.3 ± 0.3	-	-
(4 a) $U_m - U_u$ (kλ)	3.7 – 13.0	1.0 – 10.0	1.6 – 16.0	3.1 – 22.0	1.6 – 23.0	0.6 – 6.7	-	-
(5 a) $D/U_u - D/U_m$ (kpc)	0.06 – 0.27	0.8 – 8.0	0.19 – 1.9	0.18 – 1.16	0.1 – 1.3	0.56 – 6.2	-	-
(6 a) $\chi^2/\nu$	0.3	0.2	0.2	0.7	0.6	0.4	-	-
(1 b) $N$	10	64	8	12	8	16	8	8
(2 b) velocity width (km s <sup>-1</sup> )	16.5	82.56	13.2	19.8	13.2	26.4	19.8	19.8
(3 b) $\alpha$	-2.1 ± 0.6	-1.5 ± 0.2	-2.5 ± 0.4	-1.7 ± 0.4	-0.7 ± 0.3	-	-	-
(4 b) $U_m - U_u$ (kλ)	3.7 – 13.0	1.0 – 10.0	1.6 – 16.0	3.1 – 22.0	1.6 – 23.0	-	-	-
(6 a) $D/U_u - D/U_m$ (kpc)	0.06 – 0.27	0.8 – 8.0	0.19 – 1.9	0.18 – 1.16	0.1 – 1.3	-	-	-
(6 b) $\chi^2/\nu$	0.4	0.2	1.3	0.3	0.2	-	-	-
(7) $\zeta_2$	0 ± 1.2	0 ± 0.4	0 ± 0.8	0 ± 1.2	0 ± 0.8	0 ± 0.6	-	-

**Table 2.** The results for the 8 galaxies in our sample. Rows 1-6 gives (1)  $N$  the number of channels averaged over, (2) the corresponding velocity width (3)  $\alpha$  the best fit slope for the HI power spectrum, (4)  $U$  range over which the power law fit is valid, (5) length-scales over which the power law fit is valid and (6) the goodness of fit  $\chi^2$  per degree of freedom. Row (7) Possible limits for the spectral slope of the velocity structure function.

For all the galaxies we have tried to fit the observed  $P_{HI}(U)$  with a power law  $P_{HI}(U) = AU^\alpha$ . We find that this provides a good fit with a reasonable  $\chi^2/\nu$  for DDO 210, NGC 628, NGC 3741, UGC 4459, GR 8 and AND IV. The presence of a scale invariant, power law power spectrum indicates that turbulence is operational in the ISM of these galaxies. The range of length-scales for the power law fit differs from galaxy to galaxy and in total it covers 100pc to 8Kpc. The details are summarized in Table 2.

Both HI density fluctuations as well as spatial fluctuations in the velocity of the HI gas contribute to fluctuations in the HI specific intensity. Considering a turbulent ISM, Lazarian & Pogosyan (2000) have shown that it is possible to disentangle these two contributions by studying the behavior of the HI power spectrum as the thickness of the frequency channel is varied. If the observed HI power spectrum is due to the gas velocities, the slope of the power spectrum is predicted to decrease with increasing thickness of the frequency channel. To test this we have repeated the power spectrum analysis increasing the channel thickness  $N$  from  $N = 1$  to  $N = n$ . In addition to  $N = 1$ , Figures 8 and 9, and Table 2 also show the results for  $N = n$  where the channel thickness spans the entire frequency range that has significant HI emission. We do not find a significant change in the slope of the power spectrum for any of the galaxies. Since for all the galaxies the thickest channel is considerably larger than the velocity dispersion, we conclude that the HI power spectrum is purely due to density fluctuations and not gas velocities. The fact that the slope does not change with channel thickness can be used to constrain the value of  $\zeta_2$ , the slope of the

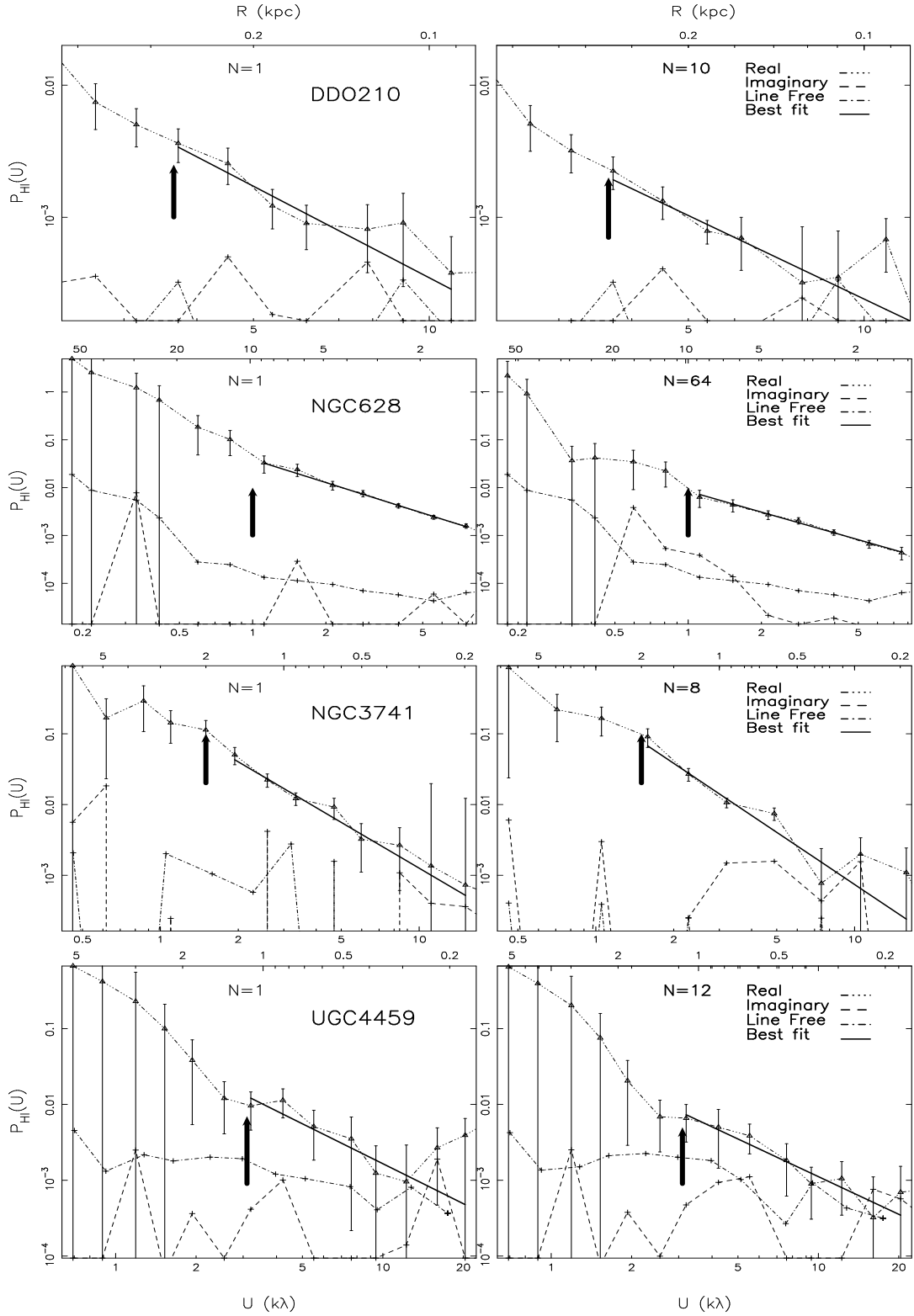


**Figure 8.** Power spectrum of the galaxies DDO 210, NGC 628, NGC 3741 and UGC 4459. The real and imaginary parts of  $\hat{P}_{\text{HI}}(U)$  estimated after averaging  $N$  channels with HI emission, and the real part from  $N$  line-free channels are shown together for  $N = 1$  (left panel) and  $N = n$  (right panel). The error-bars are for the real part from channels with HI emission. The best fit power law is shown in bold. In each case  $U_m$  is marked with a bold-faced arrow and the fit is restricted to  $U > U_m$  where the effect of the convolution with the window function can be ignored.

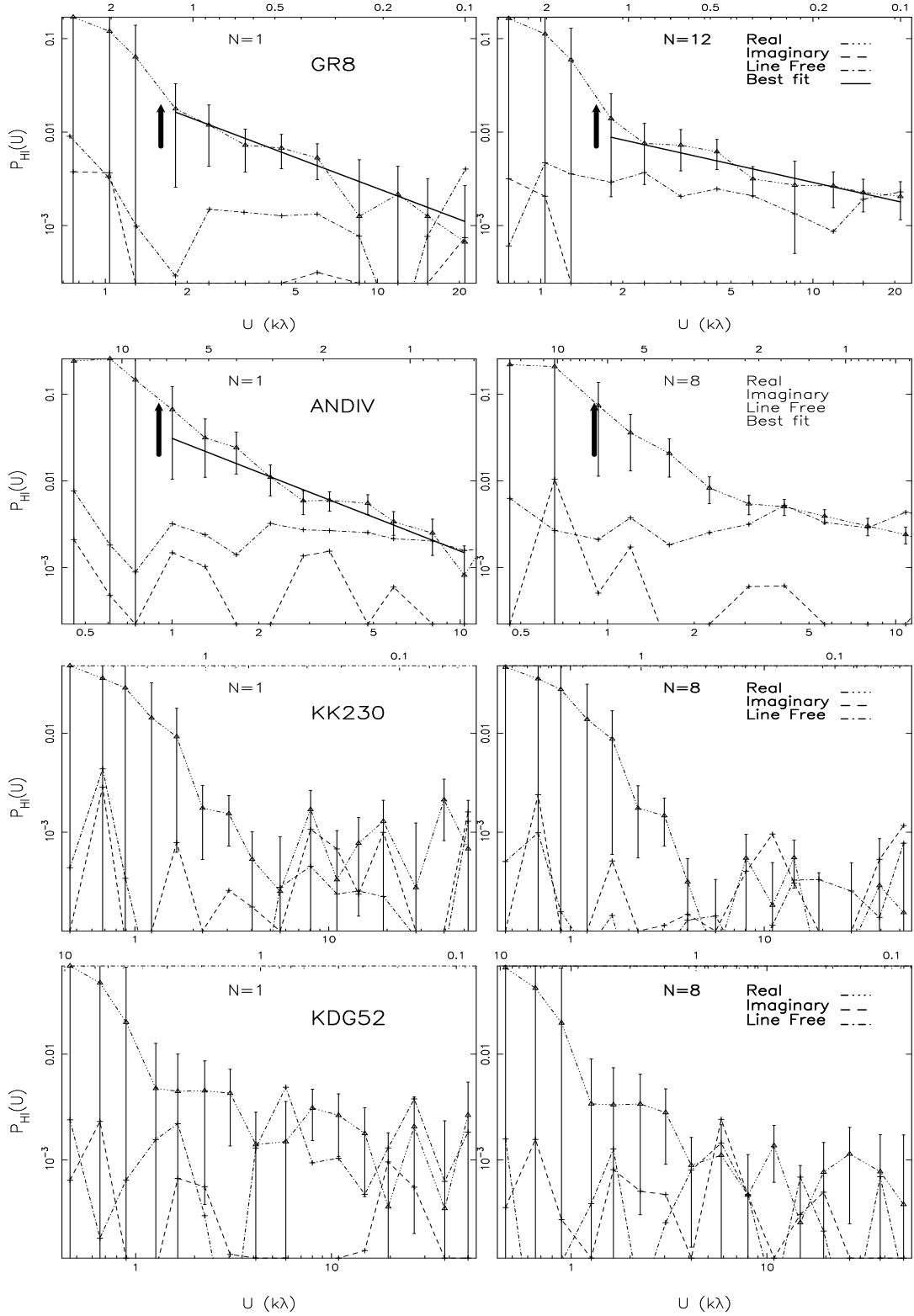


**Figure 9.** Power spectrum of the galaxies GR 8, AND IV, KK 230 and M81DWA. The real and imaginary parts of  $\hat{P}_{\text{HI}}(U)$  estimated after averaging  $N$  channels with HI emission, and the real part from  $N$  line-free channels are shown together for  $N = 1$  (left panel) and  $N = n$  (right panel). The error-bars are for the real part from channels with HI emission. The best fit power law is shown in bold only where such a fit is possible. For those,  $U_m$  is marked with a bold-faced arrow and the fit is restricted to  $U > U_m$  where the effect of the convolution with the window function can be ignored.

velocity structure function (eg. Lazarian & Pogosyan 2000). The  $\zeta_2$  values are tabulated in Table 2.

The galaxies in our sample have slope  $\alpha$  ranging from  $-2.6$  to  $-1.1$ . The two galaxies DDO 210 and NGC 3741 have slope  $\sim -2.5$ , while the slope is  $\sim -1.5$  for NGC 628, UGC 4459 and AND IV, and  $-1.1$  for GR 8. We have proposed a possible explanation for this dichotomy in the values of  $\alpha$  in Dutta et al. (2008). This was based on the fact that DDO 210, where the power spectrum was measured across length-scales  $100 - 500$  pc, had a slope of  $-2.6$  while NGC 628, a nearly face-on galaxy where the power spectrum was measured across length-scales  $0.8 - 8$  kpc had a slope of  $-1.6$ . We have interpreted the former as three dimensional (3D) turbulence operational at small scales whereas the latter was interpreted as two dimensional (2D) turbulence in the plane of the galactic disk. For a nearly face-on disk galaxy we expect the transition from 2D to 3D turbulence to be seen at a length-scale corresponding to the scale height of the galaxy. Continuing with this interpretation implies that we have also measured 3D turbulence in NGC 3741, and 2D turbulence in UGC 4459, GR 8 and AND IV.

The power spectrum analysis can be used to determine the scale-height of nearly face-on galaxies (Elmegreen et al. 2001; Padoan et al. 2001). Elmegreen et al. (2001) have applied this method to estimate the scale height of LMC. In a recent study (Dutta et al. 2008) we have placed an upper limit of  $800$  pc for the scale-height of NGC 628. Our simulations (Section 4) show that we expect the slope of the HI power spectrum to change corresponding to a transition from 3D to 2D turbulence at the scale-height. The baseline  $U$  at which this break occurs can be used to estimate the scale-height  $D/\pi U$ , where  $D$  is the distance to the galaxy.

In addition to NGC 628, our sample contains 3 more nearly face-on galaxies with  $i_{\text{HI}} < 30^\circ$ , namely DDO 210, UGC 4459 and GR 8. DDO 210 has 3D turbulence across the baselines  $2.0 - 10.0$  k $\lambda$ . The absence of a break in the power spectrum places a lower limit of  $160$  pc on the scale-height. The galaxies NGC 628, UGC 4459 and GR 8 exhibit 2D turbulence for the entire  $U$  range (Table 2) in the measured HI power spectrum. This imposes the upper limit of  $320$  pc,  $51$  pc and  $30$  pc respectively on the scale-height. Note that the scale-height of  $320$  pc for NGC 628 differs from our earlier estimate (Dutta et al. 2008) because of the extra factor of  $\pi$  indicated by our simulations.

The energy input from star formation is believed to be a major driving force for the turbulence in the ISM (Elmegren & Scalo 2004a). Hence, it is very interesting to check

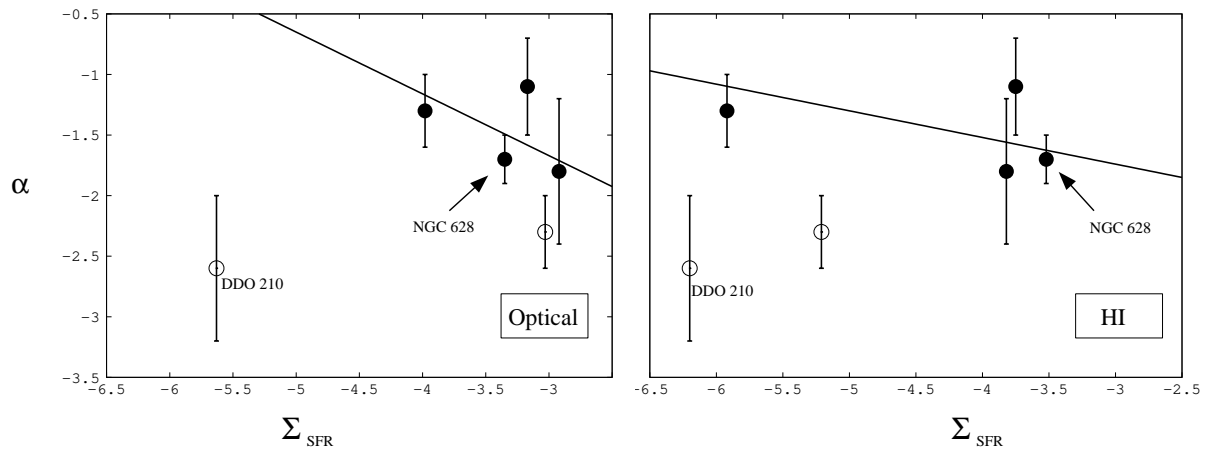


**Figure 10.** The slope  $\alpha$  of the HI power spectrum plotted against  $\Sigma_{\text{SFR}}$ , the SFR per unit area. The area has been determined from optical images and HI images in the left and right panels respectively. The galaxies with 3D and 2D turbulence are shown using empty and filled circles respectively. Note that the SFR for DDO 210, marked in the figure, is only an upper limit. The data for NGC 628, which is a spiral galaxy, is marked with an arrow. The straight lines show the linear correlation that we find (discussed in the text) between the slope of the HI power spectrum and the SFR per unit area.

whether the slope of the power spectrum of intensity fluctuations in these galaxies has any correlation with the SFR. Any correlation, if present, will provide an insight into the processes driving turbulence in the ISM.

In a recent study Willett et al. (2005) calculate the SFR per unit area for 9 irregular galaxies and investigate the correlation with the V-band and  $\text{H}\alpha$  power spectra. The length-scales they probe are 10 – 400 pc. In  $\text{H}\alpha$  they find that the power spectra becomes steeper as the SFR per unit area increases. However they do not find any correlation in the V-band. In this paper we probe length-scales 100 pc to 3.5 kpc. We test for a possible correlation between the slope of the power spectrum and the SFR per unit area and per unit HI mass for the 5 dwarf galaxies in our sample (Figure 10). We report results using the area estimated from both, the HI disk and the optical disk. The data for the SFR, angular extent, inclination in HI and HI mass for these galaxies are from Begum et al. (2005) and Begum et al. (2008). The SFR is determined from  $\text{H}\alpha$  emission, and the angular extent in HI is determined from the Moment0 maps at a column density of  $10^{19}$  atoms  $\text{cm}^{-2}$ . For the angular extent and inclination of the optical disk we use the parameters from Young et al. (2000), Begum et al. (2006) and Sharina et al. (2008). The linear correlation coefficient is found to have values 0.35 and 0.34 for the HI and optical disks respectively, indicating the absence of any correlation between the slope of the power spectrum and the SFR per unit area. We have similar result for SFR per unit HI mass for these 5 galaxies. However, we note a few points that should be taken into consideration when interpreting this conclusion. The  $\text{H}\alpha$  emission is not a good tracer of SFR in low mass galaxies due to stochastic star formation (Karachentsev & Kaisin

2007; Lee et al. 2007). Also, the length-scales across which the power spectrum has been estimated for the dwarf galaxies in our sample are substantially larger than the optical disk where star formation occurs.

Turbulence can also possibly be related to different parameters of the galaxy. We test for correlations between the slope of the HI power spectrum and the following parameters: total HI mass, HI mass to light ratio, total dynamical mass, total baryonic mass, gas fraction, baryon fraction. We use the estimates of these observable quantities from Begum et al. (2007). In all the cases the linear correlation coefficient is found to lie between  $-0.5$  and  $0.5$ , indicating the absence of correlation.

In the above analysis we have considered galaxies with both 2D and 3D turbulence taken together, which in turn can suppress the correlations. Hence, we further investigated the correlations by considering the 4 galaxies in our sample (including NGC 628) with 2D turbulence. In this case the correlation coefficient comes out to be  $-0.70$  and  $-0.74$  for SFR per unit area of optical and HI disks respectively. This indicates a strong correlation and the result is similar to that of Willett et al. (2005), namely that the surface density of star formation rate is larger for galaxies with steeper HI power spectrum. These findings indicate a possible link between star formation and the nature of turbulence in the ISM. However, it would not be realistic to speculate on a possible cause and effect relation between these two. It is quite possible that the observed correlation is an outcome of extraneous factors which influence both.

Finally, we note that the total number of galaxies in all of our analysis is rather small for a statistical conclusion. A larger galaxy sample is required for a better understanding of the generic features, if any, of turbulence in the ISM of faint dwarf galaxies.

## ACKNOWLEDGMENTS

P.D. is thank full to Sk. Saiyad Ali, Kanan Datta, Prakash Sarkar, Tapomoy Guha Sarkar, Wasim Raja and Yogesh Maan for use full discussions. P.D. would like to acknowledge SRIC, IIT, Kharagpur for providing financial support. S.B. would like to acknowledge financial support from BRNS, DAE through the project 2007/37/11/BRNS/357. Data presented in this paper were obtained from GMRT (operated by the National Centre for Radio Astrophysics of the Tata Institute of Fundamental Research) and NRAO VLA.

## REFERENCES

- Ali, S. S., Bharadwaj, S., & Chengalur, J. N. 2008, MNRAS, 385, 2166
- Begum, A., & Chengalur, J. N. 2003, AAP, 409, 879
- Begum, A., & Chengalur, J. N. 2004, AAP, 413, 525
- Begum, A., 2006, Ph.D. Thesis, TIFR deemed university.
- Begum, A., Chengalur, J. N., & Karachentsev, I. D. 2005, AAP, 433, L1
- Begum, A., Chengalur, J. N., Karachentsev, I. D., Kaisin, S. S., & Sharina, M. E. 2006, MNRAS, 365, 1220
- Begum, A., Chengalur, J. N., & Bhardwaj, S. 2006, MNRAS, 372, L33
- Begum, A., Chengalur, J. N., Kennicutt, R. C., Karachentsev, I. D., & Lee, J. C. 2007, MNRAS, 1113
- Begum, A., Chengalur, J. N., Karachentsev, I. D., Sharina, M. E., & Kaisin, S. S. 2008, MNRAS, 386, 1667
- Binney, J., & Merrifield, M. 1998, *Galactic astronomy / James Binney and Michael Merrifield*. Princeton, NJ : Princeton University Press, 1998. (Princeton series in astrophysics) QB857 .B522 1998
- Crovisier, J., & Dickey, J. M. 1983, AAP, 122, 282
- Deshpande, A. A., Dwarakanath, K. S., & Goss, W. M. 2000, APJ, 543, 227
- Dickinson et al. MNRAS353, 732
- Dutta, P., Begum, A., Bharadwaj, S., & Chengalur, J. N. 2008, MNRAS, 384, L34
- Elmegreen, B. G., Kim, S., & Staveley-Smith, L. 2001, APJ, 548, 749
- Elmegreen, B. G., & Scalo, J. 2004a, ARAA, 42, 211
- Elmegreen, B. G., Elmegreen, D. M., Chandar, R., Whitmore, B., & Regan, M. 2006, APJ, 644, 879
- Ferguson, A. M. N., Gallagher, J. S., & Wyse, R. F. G. 2000, AJ, 120, 821
- Gentile, G., Salucci, P., Klein, U., & Granato, G. L. 2007, MNRAS, 375, 199
- Green, D. A. 1993, MNRAS, 262, 327
- Hobson, Lasenby & Jones, MNRAS, 275, 863
- Hobson, & Maisinger, MNRAS334, 569
- Hodge, P. W. 1967, APJ, 148, 719
- Kamphuis, J., & Briggs, F. 1992, AAP, 253, 335
- Karachentsev, I. D., Karachentseva, V. E., Huchtmeier, W. K., & Makarov, D. I. 2004, AJ,

- 24 *Prasun Dutta, Ayesha Begum, Somnath Bharadwaj and Jayaram N. Chengalur*  
127, 2031
- Karachentsev, I. D., & Kaisin, S. S. 2007, *AJ*, 133, 1883
- Krakow, W., Huntley, J. M., & Seiden, P. E. 1982, *AJ*, 87, 203
- Kunth, D., & Östlin, G. 2000, *AAPR*, 10, 1
- Lazarian, A. 1995, *AAP*, 293, 507
- Lazarian, A., & Pogosyan, D. 2000, *APJ*, 537, 720
- Lee, M. G., Aparicio, A., Tikonov, N., Byun, Y.-I., & Kim, E. 1999, *AJ*, 118, 853
- Lee, J. C., Kennicutt, R. C., Funes, S. J., José G., Sakai, S., & Akiyama, S. 2007, *APJL*, 671, L113
- Merrett, H. R., et al. 2006, *MNRAS*, 369, 120
- Oey, M. S. 2002, *ASPC*, 276, 295
- Padoan, P., Kim, S., Goodman, A., & Staveley-Smith, L. 2001, *APJL*, 555, L33
- Persic, M., & Rephaeli, Y. 2007, *AAP*, 463, 481
- Roy, N., Bharadwaj, S., Dutta, P., & Chengalur, J. N. 2009, *MNRAS*, 393, L26
- Scalo, J., & Elmegreen, B. G. 2004b, *ARAA*, 42, 275
- Sharina, M. E., Karachentsev, I. D., & Tikhonov, N. A. 1996, *AAPS*, 119, 499
- Sharina et al. (in preparation)
- Sohn, Y. & Davidge, T. J., 1996, *AJ*, 111, 2280
- Stanimirovic, S., Staveley-Smith, L., Dickey, J. M., Sault, R. J., & Snowden, S. L. 1999, *MNRAS*, 302, 417
- Vinkó, J., et al. 2004, *AAP*, 427, 453
- Westpfahl, D. J., Coleman, P. H., Alexander, J., & Tongue, T. 1999, *AJ*, 117, 868
- White et al. *APJ*, 514, 12
- Willett, K. W., Elmegreen, B. G., & Hunter, D. A. 2005, *AJ*, 129, 2186
- Young, L. M., van Zee, L., Dohm-Palmer, R. C., & Lo, K. Y. 2000, *ArXiv Astrophysics e-prints*, arXiv:astro-ph/0009069